

Electronic Supplementary Information

Scaffold Membrane of Solid Polymer Electrolytes for Realizing High-Stability and Dendrite-Free Lithium-Metal Batteries

Hanh T. T. Nguyen,^a Dang H. Nguyen,^a Qin-Cheng Zhang,^a Yuh-Lang Lee,^{a,b} Jeng-Shiung Jan,^a Chi-Cheng Chiu,^a and Hsisheng Teng^{a,b,*}

^aDepartment of Chemical Engineering, National Cheng Kung University, Tainan 70101, Taiwan

^bHierarchical Green-Energy Materials (Hi-GEM) Research Center, National Cheng Kung University, Tainan 70101, Taiwan

*E-mail: hteng@mail.ncku.edu.tw

Supporting information for:

- (1). Schematic illustration of NSPE (Fig. S1)
- (2). Top-view SEM images of porous PVdF-HFP membranes (Fig. S2)
- (3). Side-view SEM images of porous PVdF-HFP membranes (Fig. S3)
- (4). Thermal analysis of NSPE@PF and its components (Fig. S4)
- (5). Mechanical strength analysis of NSPE@PF and its components (Fig. S5)
- (6). Photograph of NSPE-incorporated PVdF-HFP-1.5 membrane (Fig. S6)
- (7). Top-view SEM image of the NSPE@PF membrane (Fig. S7)
- (8). Crystallinity analysis of NSPE and precursor polymer (Fig. S8)
- (9). Impedance spectra of SS|NSPE@PF|SS and SS|NSPE|SS (Fig. S9)
- (10). Electrochemical analysis on solid-state symmetric Li||Li cells (Fig. S10)
- (11). Li plating/stripping of liquid-phase Li||Li cells (Fig. S11)
- (12). Performance survey of PEO-based SPEs (Table S1)
- (13). Charge–discharge profiles of Li|NSPE|LiFePO₄ (Fig. S12)
- (14). Impedance spectra of solid-state cells (Fig. S13)
- (15). Impedance analysis on interfacial capacitive behavior (Fig. S14)

(1). Schematic illustration of NSPE

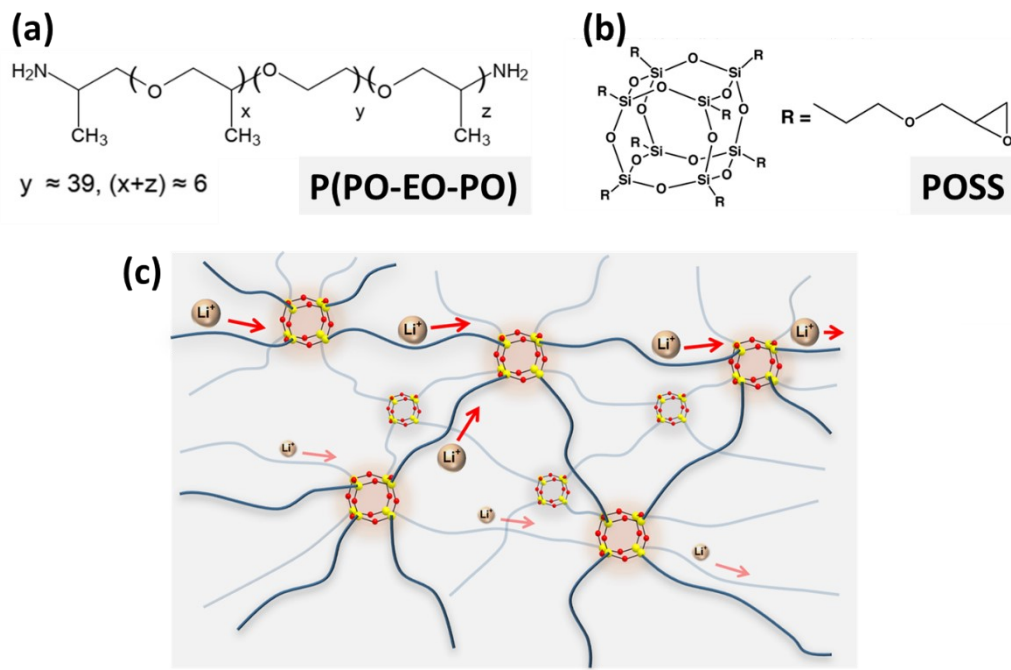


Fig. S1 Structure of the NSPE and its components. (a) A P(PO-EO-PO) polymer chain with amino ends. (b) A cage-like POSS molecule containing eight tentacles with epoxy ends. (c) The NSPE with conceptual illustration of Li^+ ion transport in the network.

(2). Top-view SEM images of porous PVdF-HFP membranes

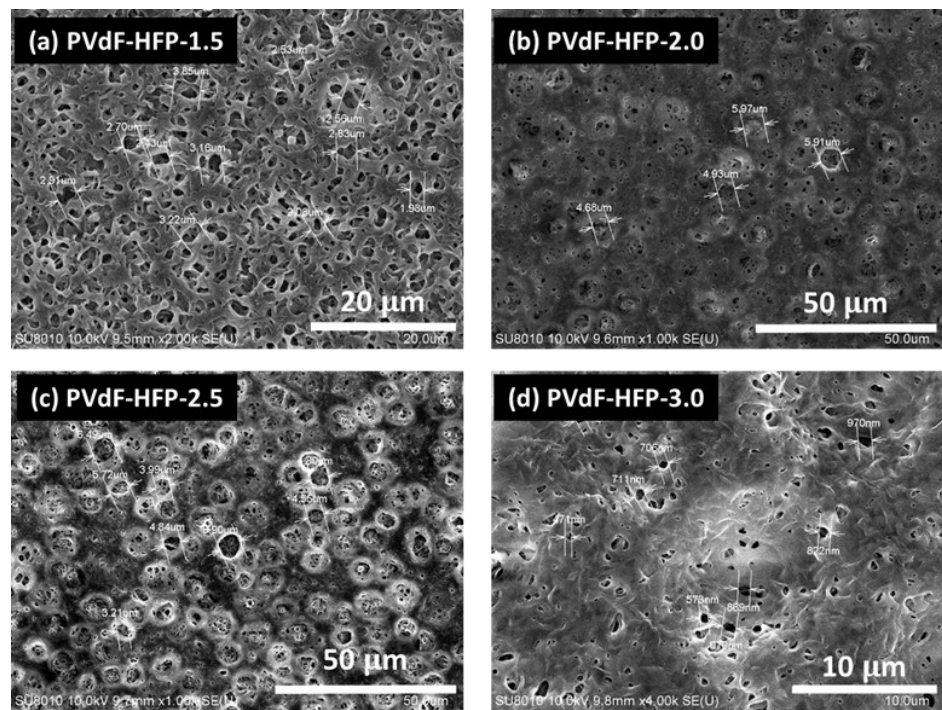


Fig. S2 Top-view SEM images of the porous PVdF-HFP membranes. (a) PVDF-HFP-1.5. (b) PVDF-HFP-2.0. (c) PVDF-HFP-2.5. (d) PVDF-HFP-3.0.

(3). Side-view SEM images of porous PVdF-HFP membranes

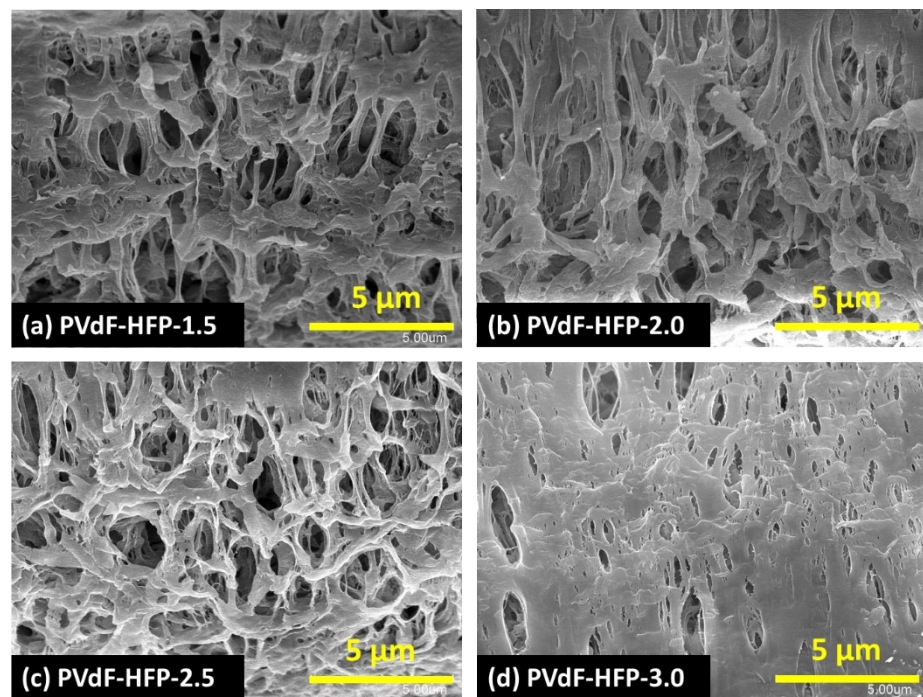


Fig. S3 Side-view SEM images of the porous PVdF-HFP membranes. (a) PVDF-HFP-1.5. (b) PVDF-HFP-2.0. (c) PVDF-HFP-2.5. (d) PVDF-HFP-3.0.

(4). Thermal analysis of NSPE@PF and its components

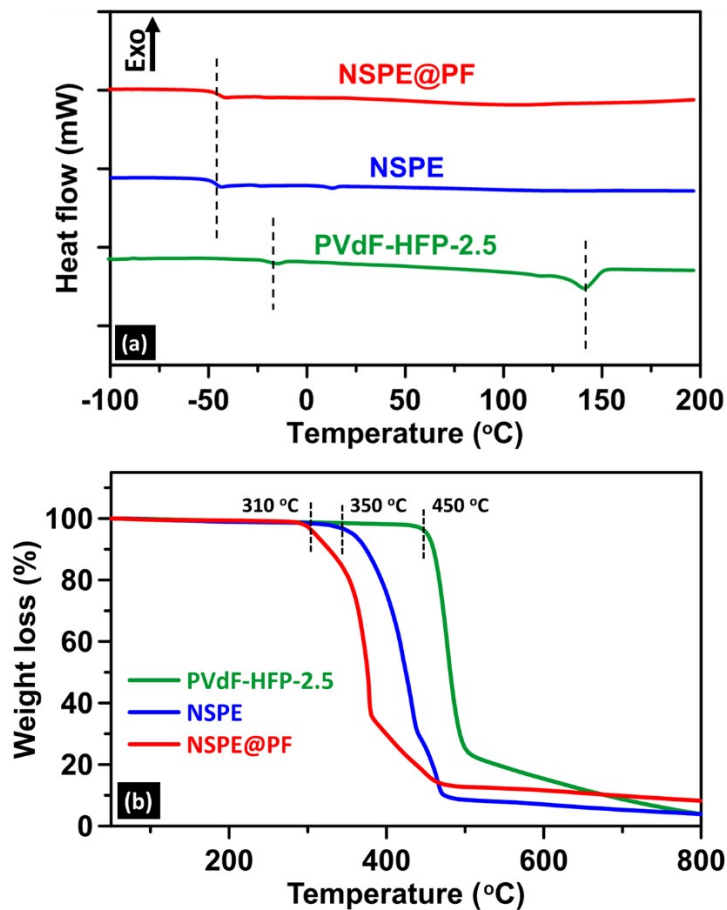


Fig. S4 Thermal analysis of the NSPE@PF membrane and its components. (a) Differential scanning calorimetry analysis of the PVdF-HFP-2.5, NSPE@PF, and NSPE membranes. (b) Thermogravimetric analysis of PVdF-HFP-2.5, NSPE@PF and NSPE membranes. Both analyses were conducted at a constant heating rate of $10\text{ }^{\circ}\text{C min}^{-1}$ under a continuous nitrogen purge.

(5). Mechanical strength analysis of NSPE@PF and its components

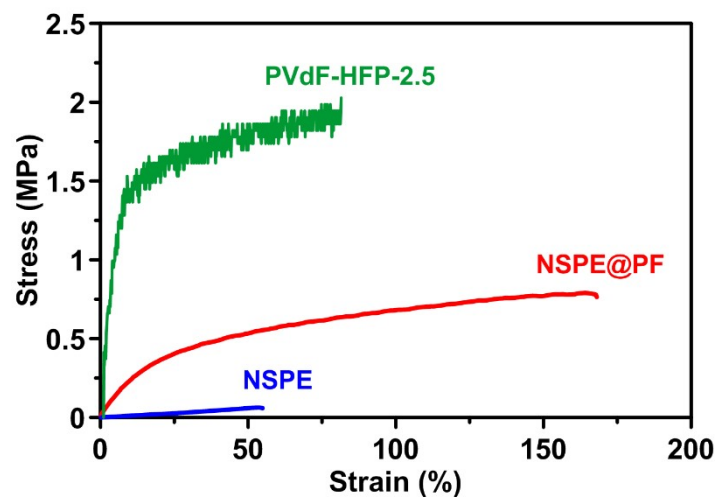


Fig. S5 Mechanical strength analysis of the PVdF-HFP-2.5, NSPE@PF, and NSPE membranes.

(6). Photograph of NSPE-incorporated PVdF-HFP-1.5 membrane



Fig. S6 Photograph of the NSPE-incorporated PVdF-HFP-1.5 membrane.

(7). Top-view SEM image of the NSPE@PF membrane

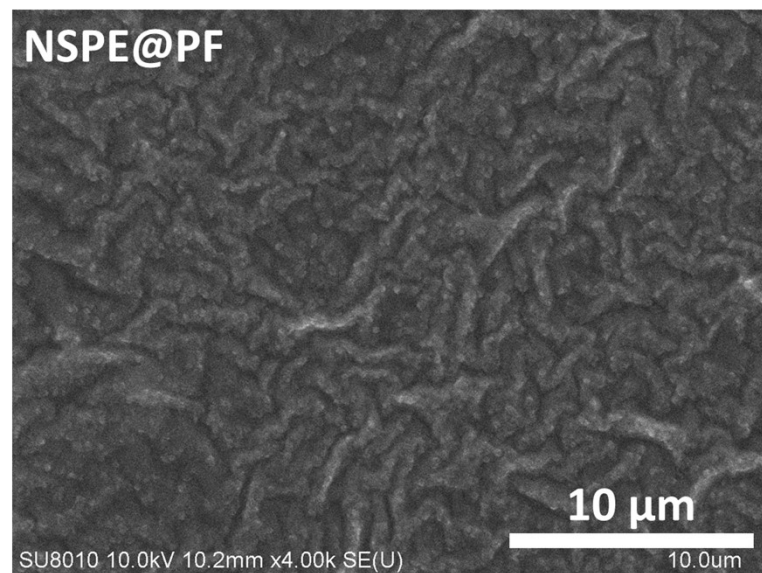


Fig. S7 Top-view SEM image of the NSPE@PF membrane.

(8). Crystallinity analysis of NSPE and precursor polymer

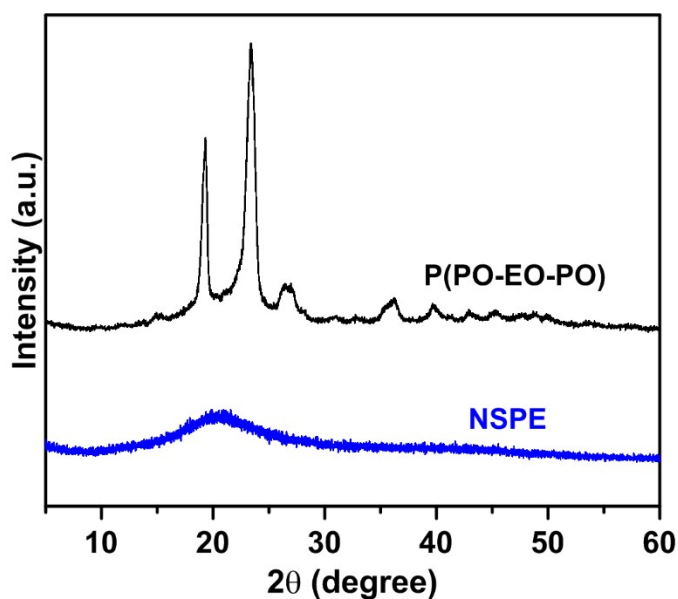


Fig. S8 X-ray diffraction patterns of the NSPE and its precursor P(PO-EO-PO).

(9). Impedance spectra of SS|NSPE@PF|SS and SS|NSPE|SS

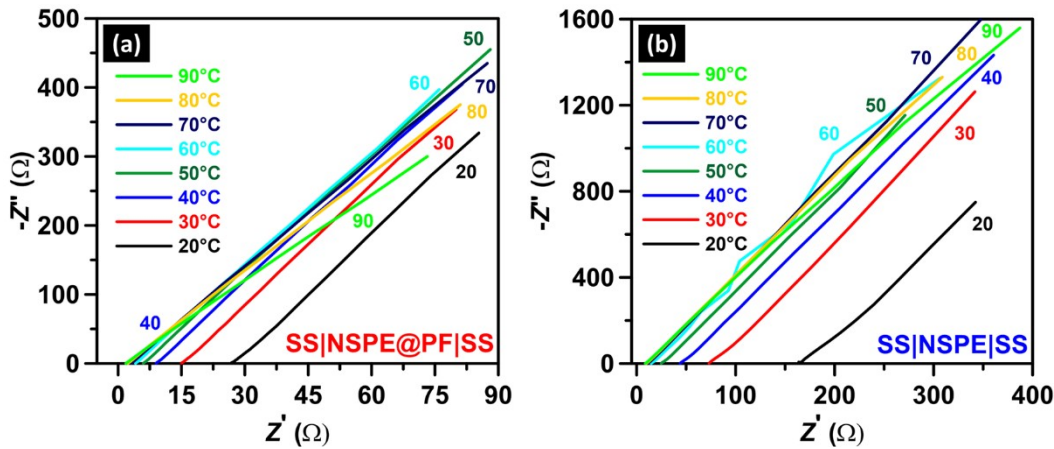


Fig. S9 Temperature dependence of the AC impedance spectra of SS||SS inserted with SPEs. (a) SS|NSPE@PF|SS. (b) SS|NSPE|SS. The NSPE@PF and NSPE membranes were sandwiched between the two stainless-steel electrodes for the impedance measurements operated measured at 0 V with an AC potential amplitude of 10 mV over a frequency range of 1 Hz to 1 MHz.

The ionic conductivity (σ) was calculated using the following equation:

$$\sigma = \frac{d}{R_I \times A}$$

where d is the distance between the SS electrodes, R_I is the bulk resistance determined from the intercept on the real axis of the impedance plot, and A is the geometric area of the electrolyte-electrode interface.

(10). Electrochemical analysis on solid-state symmetric Li||Li cells

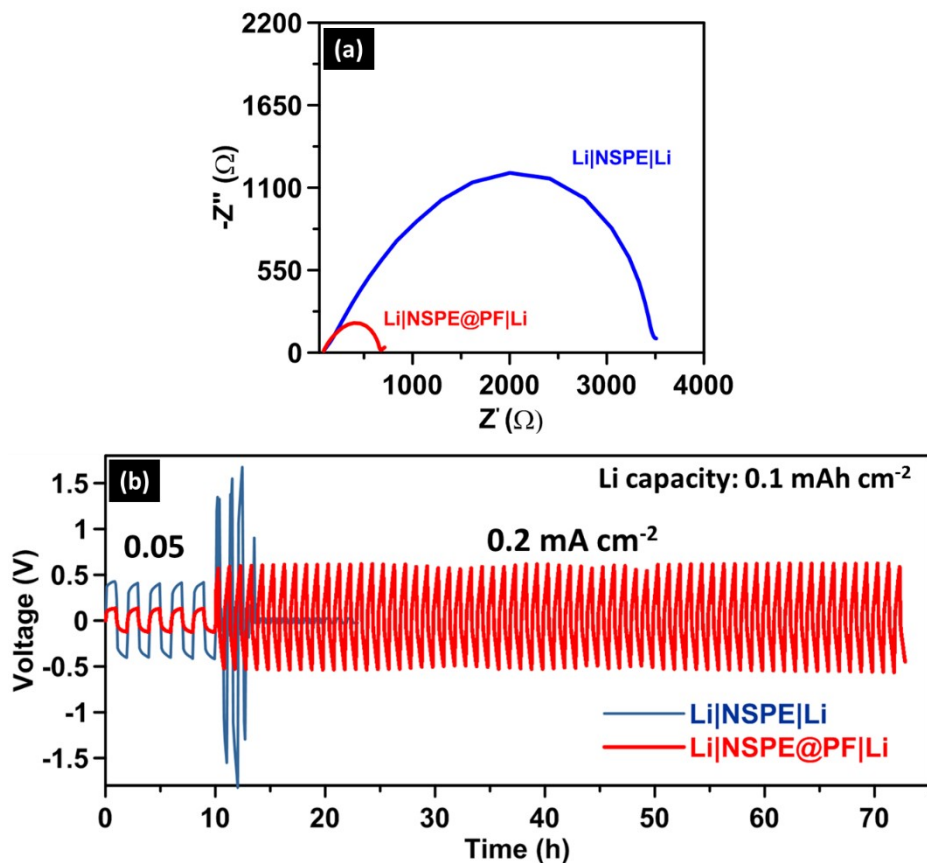


Fig. S10 Electrochemical analysis on solid-state symmetric Li||Li cells. (a) AC impedance complex-plane spectra of the $\text{Li}|\text{NSPE}@\text{PF}|\text{Li}$ and $\text{Li}|\text{NSPE}|\text{Li}$ cells. (b) Li plating/stripping voltage profiles of the $\text{Li}|\text{NSPE}@\text{PF}|\text{Li}$ and $\text{Li}|\text{NSPE}|\text{Li}$ cells at current density of $200 \mu\text{A cm}^{-2}$ with Li capacity of 0.1 mAh cm^{-2} for each step. The tests were conducted at 30°C .

(11). Li plating/stripping of liquid-phase Li||Li cells

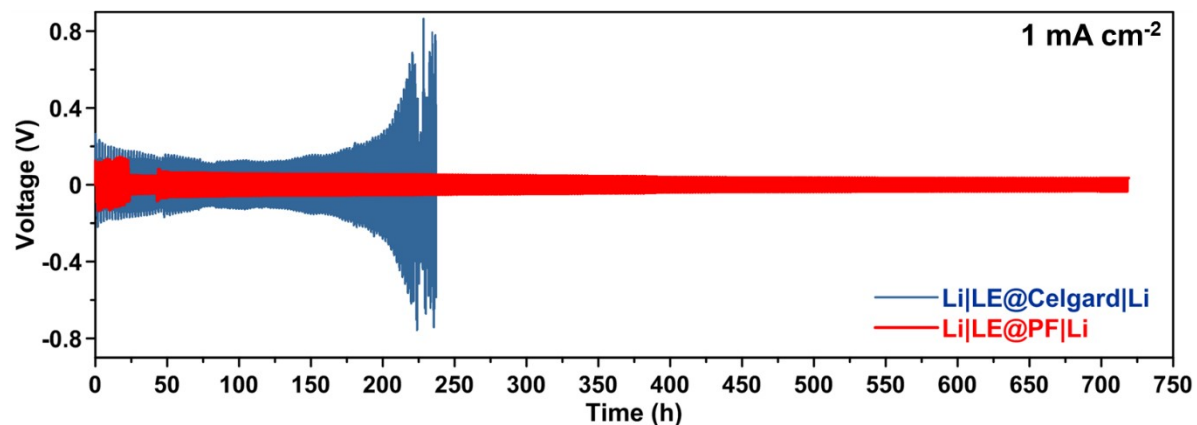


Fig. S11 Li plating/stripping profiles of the Li|LE@PF|Li and Li|LE@Celgard|Li cells at current density of 1 mA cm^{-2} with a Li capacity of 1 mAh cm^{-2} for each step. The tests were conducted at 30°C .

(12). Performance survey of PEO-based SPEs

Table S1 Literature survey on the ionic conductivity (σ) and lithium transference number (t_{Li^+}) of liquid electrolytes and PEO-based SPEs.

No.	Composition of electrolytes	σ [S cm ⁻¹]	t_{Li^+}	Ref.
1	Liquid electrolyte	-	0.20-0.40 @ 25 °C	[1]
2	PEO-based SPE	$\sim 10^{-8}$ - 10^{-6} @ 30 °C	0.2-0.3 @ 80 °C	[2, 3]
3	PEO + LiTFSI + 1% LGPS ^{a)}	1.18×10^{-5} @ 25 °C	0.26 @ 80 °C	[4]
4	PEO + LiTFSI + 10wt% LLZTO ^{b)}	3.03×10^{-4} @ 55 °C	0.117 @ 55 °C	[5]
5	PEO-TPU ^{c)} + LiTFSI	5.3×10^{-4} @ 60 °C	-	[6]
6	PEO-PS ^{d)} + LiTFSI	9.5×10^{-5} @ 60 °C	0.22 @ 60 °C	[7]
7	PEGDE ^{e)} -PEGDA ^{f)} + LiTFSI	5.3×10^{-5} @ 30 °C	0.44 @ 55 °C	[8]
8	P(PO-EO-PO) + LiTFSI	5.3×10^{-4} @ 70 °C	-	[9]
9	PEGDGE ^{g)} -PEMP ^{h)} -PDMS ⁱ⁾ + LiTFSI	3.59×10^{-5} @ 60 °C	0.20 @ 60 °C	[10]
10	PEGDMA ^{j)} -PEGDA + PETMP ^{k)} cross-linker + LiTFSI	5.05×10^{-5} @ RT ^{q)}	0.312 @ 60 °C	[11]
11	PEGA ^{l)} + SSH ^{m)} cross-linker + LiTFSI	1.78×10^{-4} @ 80 °C	0.32 @ 60 °C	[12]
12	PEEC ⁿ⁾ + TEGDA ^{o)} cross-linker	1.6×10^{-5} @ RT	0.40 @ 55 °C	[13]
13	INSPE ^{p)} + LiTFSI	5.6×10^{-5} @ 25 °C	0.37 @ 60 °C	[14]
14	P(PO-EO-PO) + PVdF-HFP scaffold	1.1×10^{-4} @ 30 °C	0.45 @ 30 °C	This work

^{a)}Li₁₀GeP₂S₁₂; ^{b)}Li_{6.75}La₃Zr_{1.75}Ta_{0.25}O₁₂; ^{c)}thermoplastic polyurethane; ^{d)}polystyrene; ^{e)}poly(ethylene glycol) diglycidyl ether; ^{f)}poly(ethylene glycol) diacrylate; ^{g)}poly(ethylene glycol) diglycidyl ether; ^{h)}pentaerythritol tetrakis (3-mercaptopropionate); ⁱ⁾poly(dimethylsiloxane); ^{j)}poly(ethylene glycol) methyl ether methacrylate; ^{k)}pentaerythritol tetra(3-mercaptopropionate); ^{l)}poly(ethylene glycol) methyl ether acrylate; ^{m)}1,2-bis(ureidoethylenemethacrylateethyl) disulfide; ⁿ⁾poly(ethylene ether carbonate); ^{o)}tetraethyleneglycol diacrylate; ^{p)}interpenetrating network polymer electrolyte; ^{q)}room temperature.

(13). Charge–discharge profiles of Li|NSPE|LiFePO₄

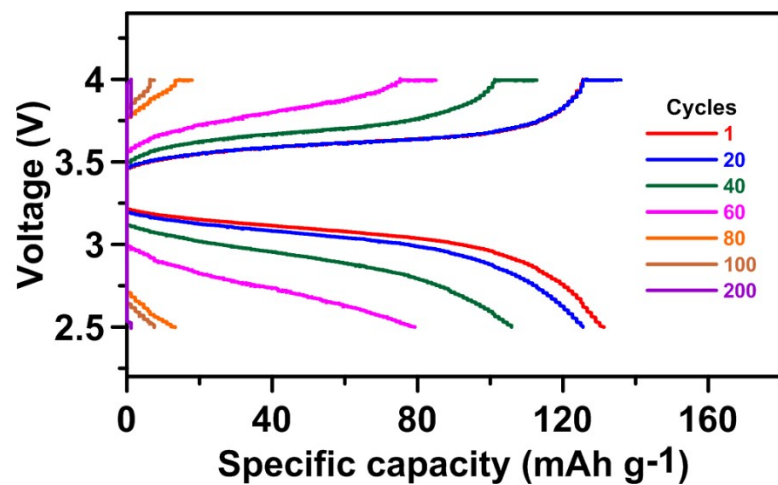


Fig. S12 Charge–discharge profiles of the Li|NSPE|LiFePO₄ battery at different cycles for cycling at 0.3C and 30 °C.

(14). Impedance spectra of solid-state cells

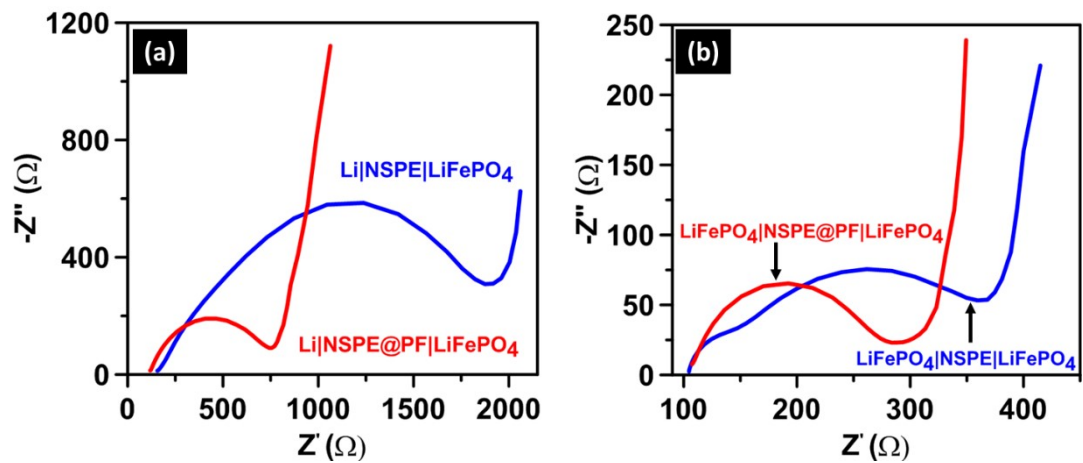


Fig. S13 AC impedance complex-plane spectra of solid-state cells. (a) $\text{Li}|\text{NSPE}@\text{PF}|\text{LiFePO}_4$ and $\text{Li}|\text{NSPE}| \text{LiFePO}_4$. (b) $\text{LiFePO}_4|\text{NSPE}@\text{PF}|\text{LiFePO}_4$ and $\text{LiFePO}_4|\text{NSPE}| \text{LiFePO}_4$.

(15). Impedance analysis on interfacial capacitive behavior

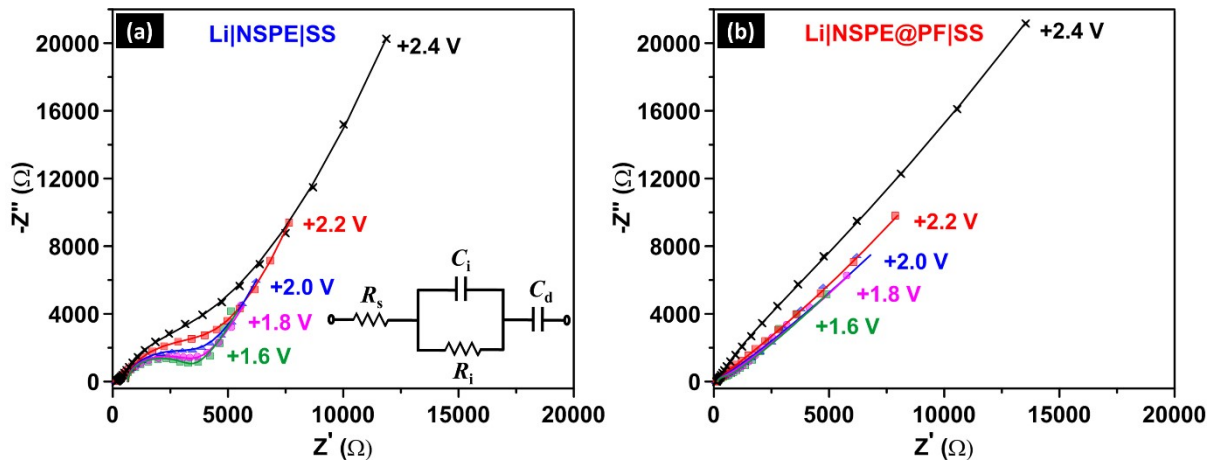


Fig. S14 AC impedance analysis of Li|NSPE|SS and Li|NSPE@PF|SS under different applied potentials. (a) Li|NSPE|SS. (b) Li|NSPE@PF|SS. The points are the experimental data and the fitting curves were obtained from simulation using the equivalent circuit shown in the inset of panel (a). The impedance analysis was conducted with an AC amplitude of 10 mV and frequency ranging from 100 kHz to 0.1 Hz.

References

- [1] K. Xu, *Chem. Rev.*, 2004, **104**, 4303.
- [2] J. W. Fergus, *J. Power Sources*, 2010, **195**, 4554.
- [3] H. Zhang, C. Liu, L. Zheng , F. Xu, W. Feng, H. Li, X. Huang, M. Armand, J. Nie, Z. Zhou, *Electrochim. Acta*, 2014, **133**, 529.
- [4] Y. Zhao, C. Wu, G. Peng, X. Chen, X. Yao, Y. Bai, F. Wu, S. Chen, X. Xu, *J. Power Sources*, 2016, **301**, 47.
- [5] H. Zhuang, W. Ma, J. Xie, X. Liu, B. Li, Y. Jiang, S. Huang, Z. Chen, B. Zhao, *Journal of Alloys and Compounds*, 2021, **860**, 157915.
- [6] C. Tao, M. H. Gao, B. H. Yin, B. Li, Y. P. Huang, G. Xu, J. J. Bao, *Electrochim. Acta*, 2017, **257**, 31.
- [7] Y. Chen, Y. Shi, Y. Liang, H. Dong, F. Hao, A. Wang, Y. Zhu, X. Cui, Y. Yao, *ACS Appl. Energy Mater.*, 2019, **2**, 1608.
- [8] H. Duan, Y. X. Yin, X. X. Zeng, J. Y. Li, J. L. Shi, Y. Shi, R. Wen, Y. G. Guo, L. J. Wan, *Energy Storage Mater.*, 2018, **10**, 85.
- [9] I. Aldalur, H. Zhang, M. Piszcza, U. Oteo, L. M. Rodriguez-Martinez, D. Shanmukaraj, T. Rojo, M. Armand, *J. Power Sources*, 2017, **347**, 37.
- [10] M. S. Grewal, M. Tanaka, H. Kawakami, *Electrochim. Acta*, 2019, **307**, 148.
- [11] Z. Wei, S. Chen, J. Wang, Z. Wang, Z. Zhang, X. Yao, Y. Deng, X. Xu, *J. Mater. Chem. A*, 2018, **6**, 13438.
- [12] Y. H. Jo, S. Li, C. Zuo, Y. Zhang, H. Gan, S. Li, L. Yu, D. He, X. Xie, Z. Xue, *Macromolecules*, 2020, **53**, 1024.
- [13] Y. C. Jung, M. S. Park, D. H. Kim, M. Ue, A. Eftekhari, D. W. Kim, *Sci. Rep.*, 2017, **7**, 17482.
- [14] Y. Tong, H. Lyu, Y. Xu, B. P. Thapaliya, P. Li, X. G. Sun, S. Dai, *J. Mater. Chem. A*, 2018, **6**, 14847.